BIN1 knockdown rescues systolic dysfunction in the aging heart

Maartje Westhoff Ph.D.[1]*, Silvia G. del Villar Ph.D.[1]*, Taylor L. Voelker[1] Ph.D., Phung N. Thai Ph.D.[2,3], Nipavan Chiamvimonvat M.D.[2,3,4], Eamonn J. Dickson Ph.D.[1], and Rose E. Dixon Ph.D.[1]

** These authors contributed equally to this work.*

[1]Department of Physiology and Membrane Biology, University of California Davis, Davis, CA, USA

[2]Division of Cardiovascular Medicine, Department of Internal Medicine, University of California, Davis, Davis, CA, USA

[3]Department of Veterans Affairs, Northern California Health Care System, Mather, CA, USA

[4]Department of Pharmacology, University of California Davis, Davis, CA, USA

MW: https://orcid.org/0000-0002-5421-8609
SGdV: https://orcid.org/0000-0002-5612-4761
TLV: https://orcid.org/0000-0002-6779-9350
PNT: https://orcid.org/0000-0001-7344-150X
NC: https://orcid.org/0000-0001-9499-8817
EJD: https://orcid.org/0000-0001-8619-7630
RED: https://orcid.org/0000-0003-0655-690X

Corresponding author: Rose E. Dixon, redickson@ucdavis.edu Department of Physiology and Membrane Biology, 4112 Tupper Hall, One Shields Avenue, University of California Davis, Davis, CA 95616, USA

Abstract word count: 150

Main text word count (Introduction, Results, and Discussion): 5083

Abstract

Cardiac dysfunction is a hallmark of aging in humans and mice. Here we report that a two-week treatment to restore youthful Bridging Integrator 1 (BIN1) levels in the hearts of 24-month-old mice rejuvenated cardiac function and substantially reversed the aging phenotype. Our data indicate that age-associated overexpression of BIN1 occurs alongside dysregulated endosomal recycling and disrupted trafficking of cardiac $Ca_V1.2$ and type 2 ryanodine receptors. These deficiencies affect channel function at rest and their upregulation during acute stress. *In vivo* echocardiography revealed reduced systolic function in old mice. BIN1 knockdown using an adeno-associated virus serotype 9 packaged shRNA-mBIN1 restored the nanoscale distribution and clustering plasticity of ryanodine receptors and recovered Ca^{2+} transient amplitudes and cardiac systolic function toward youthful levels. Enhanced systolic function correlated with increased phosphorylation of the myofilament protein cardiac myosin binding protein-C. These results reveal BIN1 knockdown as a novel therapeutic strategy to rejuvenate the aging myocardium.

Keywords:

Calcium channels, ryanodine receptors, aging, $Ca_V1.2$, BIN1, *β*-adrenergic receptors, EC-coupling, clustering, cardiac myosin binding protein-C, cardiac troponin I

Graphical Abstract

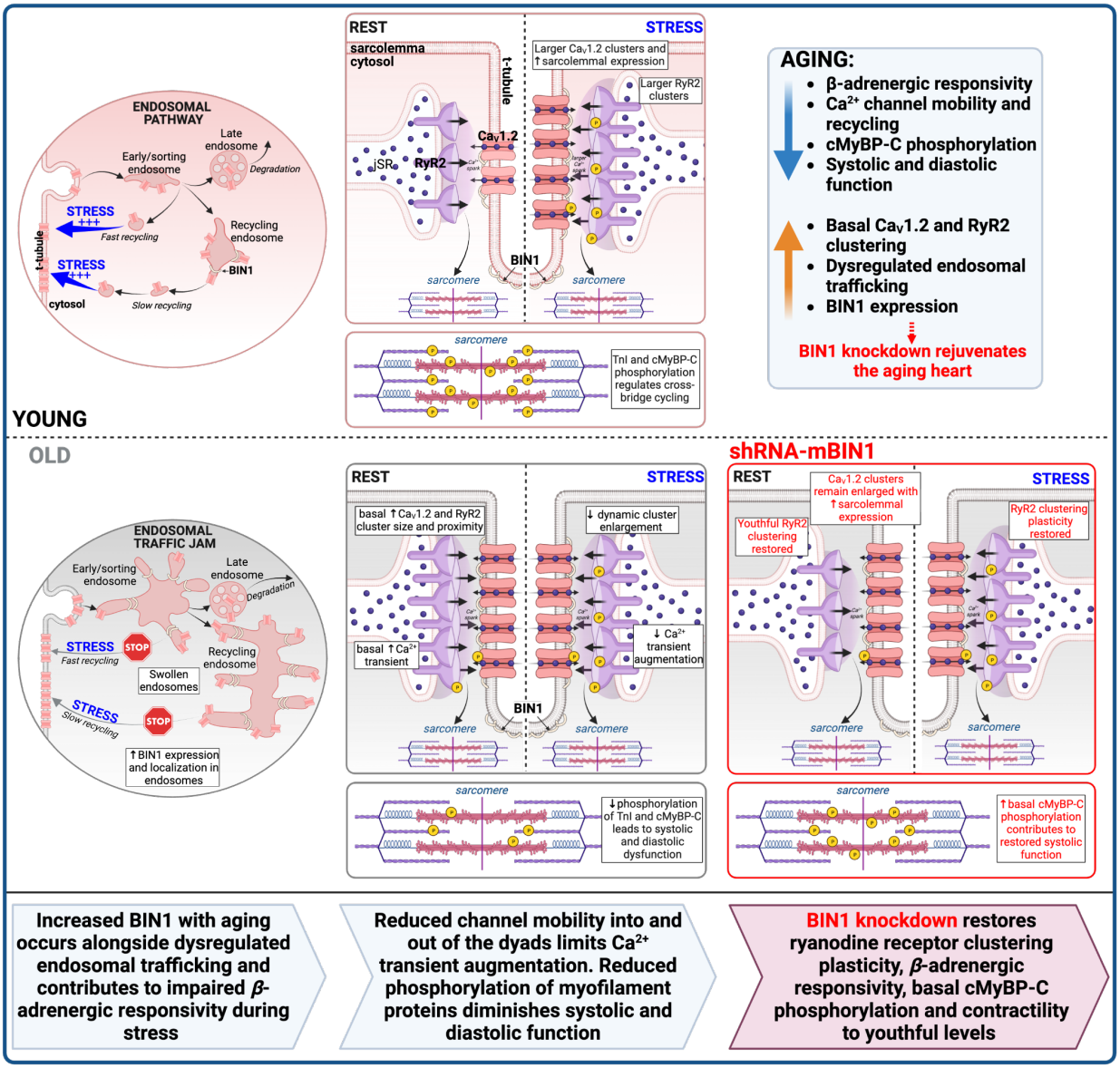

53 **Introduction**

54 Old age is a major independent risk factor for cardiovascular disease which remains the
55 leading cause of death globally[1,2]. As humans advance into old age, regardless of overall health,
56 certain intrinsic and progressive changes in cardiac structure and function occur including
57 enhanced atrial and ventricular fibrosis, left ventricular hypertrophy, and diastolic dysfunction[3-5].
58 Maximal systolic function is also impaired due to a reduced responsiveness to sympathetic
59 nervous system activation and subsequent *β*-adrenergic receptor (*β*-AR) signaling[3-5]. The decline
60 of this reactive stimulus can precipitate exercise intolerance in the elderly and render the heart
61 more vulnerable to damage during acutely stressful events when hypoxia and metabolic stress
62 ensue[4,6]. In mice, similar intrinsic cardiac changes occur over a much shorter lifespan and in the
63 absence of other risk factors like smoking or diabetes, making mice a useful model to understand
64 the molecular mechanisms of cardiac aging[3].

65 The force of myocardial contraction and the rate and extent of the subsequent relaxation
66 are tuned by both Ca^{2+} and myofilament-dependent processes. Examination and comparison of
67 these points of regulation and their integration in the *in vivo* function of young and old mice may
68 identify targets to improve the cardiac aging phenotype. Weakened myocardial contractile
69 responses to *β*AR-stimulation have been linked to an age-associated decrease in the ability of
70 the *β*AR signaling cascade to augment intracellular Ca^{2+} transient amplitude[7,8]. This has been
71 attributed to a reduced capacity to increase $Ca_V1.2$ activity and availability, and thus to diminished
72 Ca^{2+} influx during the action potential (AP)[5]. Activation of cAMP-dependent protein kinase A
73 (PKA), downstream of *β*-AR stimulation, leads to phosphorylation of the channel complex[9,10],
74 removing an inhibitory brake[11,12] and resulting in increased channel open probability (P_o) due to
75 potentiation of longer-duration 'mode 2' openings[13], and an increased number of functional
76 channels[14,15]. We recently reported that *β*-AR activation also mobilizes a sub-sarcolemmal pool
77 of $Ca_V1.2$ channels, triggering a PKA-dependent, dynamic increase in sarcolemmal $Ca_V1.2$
78 expression in ventricular myocytes[15,16]. Consequent enlargement of $Ca_V1.2$ channel clusters

79 facilitates cooperative channel interactions[16,17], and contributes to an amplification of Ca^{2+} influx
80 that rapidly tunes excitation-contraction (EC)-coupling to meet increased hemodynamic and
81 metabolic demands. We hypothesized that loss of this rheostatic mechanism in aging myocytes
82 could impose a narrow inotropic dynamic range on the system, limiting the response to *β*-AR
83 stimulation.

84 Nanoscale redistribution and augmentation of cardiac Ca^{2+} channel clustering in response
85 to *β*-AR stimulation also extends to RyR2. Accordingly, acute treatment with the *β*AR-agonist
86 isoproterenol (ISO) or a phosphorylation-inducing cocktail promotes enhanced RyR2 cluster
87 sizes[18,19], as recently reviewed[20]. This dynamic redistribution of RyR2 into larger clusters is
88 orchestrated by bridging integrator 1 (BIN1)[18] and is linked to increased Ca^{2+} spark frequency
89 which summate to produce larger Ca^{2+} transients[19,21]. There is widespread agreement that *β*-AR
90 stimulated Ca^{2+} transient augmentation is impaired in the aging myocardium[5,8], however the
91 underlying mechanisms are not understood.

92 Here, we present a comprehensive examination of cardiac Ca^{2+} channel function, their
93 nanoscale distribution, and ISO-stimulated redistribution to test the central hypothesis that age-
94 dependent disruption in the basal and on-demand trafficking and clustering of these channels
95 restricts EC-coupling plasticity during myocardial aging and contributes to the pathophysiology of
96 cardiac aging. We report that old myocytes exhibit basal super-clustering of both $Ca_V1.2$ and
97 RyR2, with no additional dynamic response to ISO. We link these deficits in cardiac Ca^{2+} channel
98 recycling and mobility to an age-associated upregulation in BIN1 and the development of
99 endosomal trafficking deficits or "endosomal traffic jams". Crucially, we find that shRNA-mediated
100 knockdown of BIN1 in old animals restores a young phenotype by re-establishing RyR2
101 organization, Ca^{2+} transient amplitude and their *β*-AR stimulated augmentation, and rejuvenating
102 myofilament protein phosphorylation levels to recover youthful systolic function.
103

104 **Results**

105 ***β-AR stimulated I_{Ca} augmentation is diminished in aging***

106 We began our study with an investigation into the $Ca_V1.2$ channel response to *β*-AR stimulation
107 by recording whole-cell Ca^{2+} currents (I_{Ca}) from 3-month-old and 24-month-old (henceforth
108 referred to as young and old, respectively) ventricular myocytes under control and 100 nM ISO-
109 stimulated conditions. In young myocytes, ISO elicited a 1.59-fold increase in peak I_{Ca} density
110 (Fig. 1a-b, and Supplementary Table 1). However, old myocytes exhibited a blunted response
111 showing only a 1.19-fold increase with ISO and basal currents were significantly larger in old
112 myocytes than in young controls (Fig. 1a-c). The maximal ISO-stimulated current amplitude was
113 similar in young and old myocytes (Fig. 1c), suggesting that the "ceiling" was intact but that the
114 "floor" or baseline shifted with aging leaving less scope for current augmentation with acute
115 adrenergic stress. Given the reduced ISO-stimulated current augmentation, these data suggest
116 a reduced *β*-adrenergic responsiveness in old mice versus young.

117

118 ***Reduced capacity of β-AR stimulation to tune EC-coupling in aging myocytes***

119 Influx of Ca^{2+} through $Ca_V1.2$ channels during AP-mediated depolarization stimulates Ca^{2+}-
120 induced Ca^{2+}-release from cross-dyad RyR2 to initiate EC-coupling. The amplitude of the
121 resultant Ca^{2+} transient largely dictates the magnitude of myocardial contraction and the fraction
122 of blood ejected, assuming constant Ca^{2+} sensitivity of the myofilaments. *β*-AR stimulation
123 enhances both $Ca_V1.2$ and RyR2-mediated Ca^{2+} influx to produce positive inotropy and a greater
124 ejection fraction. We thus examined Ca^{2+} transients in young and old myocytes to investigate the
125 effects of aging on *β*-AR tuning of EC-coupling. Transients evoked from Fluo-4AM-loaded
126 myocytes paced at 1 Hz exhibited a 4.6 ± 0.4-fold enhancement in amplitude with ISO in young
127 cells (Fig. 1d-f). In a parallel with the I_{Ca} results, basal Ca^{2+} transients in aging myocytes were
128 larger than in young myocytes (Fig. 1d and f) and the fold-increase with ISO was almost halved

129 (2.1 ± 0.3-fold change; Fig. 1e). These results further suggest reduced *β*-adrenergic
130 responsiveness in old hearts and diminished myocardial responses to acute stress.
131
132 ***Age-dependent alterations in nanoscale distribution and clustering of $Ca_V1.2$ channels***
133 Increased sarcolemmal $Ca_V1.2$ channel expression and clustering at rest in aging cells could
134 explain the age-dependent increase in basal I_{Ca}. Furthermore, the reduced responsivity to ISO
135 could be explained by an impaired capacity to mobilize/recycle additional endosomal $Ca_V1.2$
136 channels in aging myocytes. In young cells, the result of ISO-stimulated channel recycling can be
137 observed as $Ca_V1.2$ super-clustering in single molecule localization microscopy (SMLM)[15]. To
138 determine whether ISO-stimulated recycling was still functional in aging myocytes, we examined
139 the nanoscale distribution and clustering of $Ca_V1.2$ in t-tubule and crest regions of young and old
140 myocytes using super-resolution SMLM with and without ISO-stimulation. These experiments
141 confirmed that the super-clustering response to ISO was intact in the t-tubules of young myocytes,
142 where $Ca_V1.2$ channel cluster areas in ISO-treated young myocytes were 28.8% larger than
143 unstimulated controls. However, in old myocytes, channels were already basally super-clustered,
144 showed no augmentation in area with ISO, and were similarly sized to clusters in ISO-stimulated
145 young cells (Fig. 2a-b). This phenomenon was isolated to the t-tubules as crest $Ca_V1.2$
146 populations showed no significant alteration in cluster area (Supplementary Fig. 1). Overall, the
147 age-dependent increase in basal $Ca_V1.2$ channel cluster area and failure to elicit any additional
148 increase with ISO suggests that a larger number of channels are already present in old myocyte
149 t-tubule sarcolemma and that the ISO-stimulated channel insertion response is impaired in aging.
150
151 ***Age-dependent alterations in nanoscale distribution and clustering of RyR2 channels***
152 Other groups have reported a similar phosphorylation-induced cluster size expansion of the cross-
153 dyad RyR2s in young ventricular myocytes[18,19]. In agreement with those reports, SMLM
154 performed on young myocytes immunostained against RyR2, revealed that average RyR2 cluster

155 size grew by 32.7% in young myocytes after acute ISO treatment (Fig. 2c-d). However, mean
156 RyR2 cluster areas in unstimulated old myocytes were similarly sized to the expanded clusters
157 observed in ISO-stimulated young myocytes and did not undergo any further expansion with ISO.
158 These findings suggest that the ISO-stimulated nanoscale redistribution of RyR2 is also impaired
159 in aging.
160
161 ***ISO-stimulated enhancement of $Ca_V1.2$-RyR2 interactions is absent in aging***
162 Since functional crosstalk between $Ca_V1.2$ and RyR2 is an essential requirement for cardiac EC-
163 coupling, we next examined the number of sites of proximity between $Ca_V1.2$ and RyR2 using a
164 proximity ligation assay (PLA). In this assay, a fluorescent signal is emitted at each location where
165 $Ca_V1.2$ and RyR2 come within 40 nm of each other[22]. In young myocytes, acute ISO treatment
166 triggered the emergence of more $Ca_V1.2$-RyR2 proximity sites (Fig. 2e-f). This phenomenon was
167 not observed in old myocytes, where the number of $Ca_V1.2$-RyR2 proximity sites appeared to
168 have already reached a maximal level in the absence of any exogenous stimulation.
169
170 ***Dynamic TIRF imaging reveals reduced ISO-stimulated $Ca_V1.2$ insertion in aging***
171 The basal super-clustering and absence of an additional response to ISO in old myocytes may
172 indicate: (i) the endosomal reservoir is empty after already being recycled and inserted; and/or (ii)
173 the trafficking and mobilization of channels is somehow impaired by aging. To interrogate these
174 hypotheses, we visualized real-time dynamics of the channels utilizing a $Ca_V1.2$ "biosensor"
175 approach pioneered by our lab. In this technique, adeno-associated virus serotype 9 (AAV9)-
176 $Ca_V\beta_2$-paGFP auxiliary subunits are transduced via retro-orbital injections and then visualized in
177 isolated myocytes using TIRF microscopy as previously described[15,16]. The relative balance
178 between insertion and endocytosis dictates the overall expression of any membrane protein. An
179 insertion-heavy mismatch between them will lead to increased membrane expression of the
180 protein, while an endocytosis-heavy mismatch will favor reduced expression over time. We used

181 image math to calculate the relative population of channels that were inserted during the ISO
182 treatment, removed/endocytosed, or that remained static during the whole recording. As expected
183 based on our previous studies[15,16], young myocytes responded to ISO by inserting more $Ca_V1.2$
184 channels into the sarcolemma than they endocytosed, resulting in a net change in $Ca_V\beta_2$-paGFP
185 in the TIRF footprint that on average amounted to 18% (Fig. 3a, c-g). However, old myocytes
186 exhibited a comparatively blunted response with fewer ISO-stimulated insertions (Fig. 3b-c) and
187 a larger population of static channels in the TIRF footprint suggesting impaired mobility (Fig. 3e).
188 Consequently, the ISO-induced change in TIRF footprint $Ca_V\beta_2$-paGFP amounted to only 9.5%
189 (Fig. 3g). Overall, these data reveal an age-dependent deficit in ISO-triggered insertion of $Ca_V1.2$,
190 and a shift towards reduced channel mobility or "stranding" at the plasma membrane.
191
192 ***Endosomal traffic jams impede mobilization of endosomal $Ca_V1.2$ reservoirs in aging***
193 We further investigated the effects of aging on the endosomal reservoir and capacity to mobilize
194 $Ca_V1.2$ channel cargo in response to ISO by examining EEA1-positive early endosome, and
195 Rab11-positive recycling endosome pools of $Ca_V1.2$ in young and old myocytes. Accordingly,
196 Airyscan super-resolution imaging on young myocytes revealed immunostained $Ca_V1.2$ on
197 14.89% of EEA1 positive pixels (Fig. 4a-b). As we have previously reported, *β*-AR activation
198 stimulates the recycling of a portion of the early endosome $Ca_V1.2$ to the plasma membrane via
199 the Rab4-choreographed fast endosomal recycling pathway[15]. This was evidenced by a
200 significant decrease in the % colocalization between EEA1 and $Ca_V1.2$ after ISO in young
201 myocytes. In old myocytes, there was a trending increase in the percentage of EEA1/$Ca_V1.2$
202 colocalization in unstimulated cells and no ISO-induced endosomal emptying, suggesting
203 trafficking alterations (Fig. 4b). Supporting this idea, EEA1-positive early endosomes were
204 discernibly and quantifiably larger in old myocytes than in young (Fig. 4a and c).
205 Recycling deficiencies extended into Rab11-positive recycling endosomes where a similar
206 age-dependent absence of ISO-induced emptying of their $Ca_V1.2$ cargo was observed in Rab11

207 and $Ca_V1.2$ double-stained myocytes (Fig. 4d-e). Recycling endosomes were also found to be
208 significantly enlarged in old myocytes compared to young (Fig. 4f). Rab7 positive late endosomes
209 did not display any age-dependent alterations in their size or $Ca_V1.2$ cargo suggesting that the
210 degradation pathway may be intact (Supplementary Fig. 2).
211
212 ***BIN1 is overexpressed and mislocalized in old myocytes***
213 Endosomal enlargement has been linked to endosomal dysfunction and deficiencies in membrane
214 protein recycling in Alzheimer's disease (AD)[23]. Endosome swelling results from an imbalance in
215 cargo coming into and leaving endosomes, sometimes referred to as endosomal traffic jams[24].
216 BIN1/amphiphysin II has been implicated as playing a role in the development of endosomal traffic
217 jams in AD-stricken neurons[24]. In the heart, BIN1 is better known for its role in targeted delivery
218 of $Ca_V1.2$[25,26], t-tubule biogenesis[27], micro-folding[28], and maintenance[29], and in dyad formation[30].
219 However, in neurons, where there are no t-tubules, BIN1 is known to play a role in mediating
220 endosomal membrane curvature and tubule formation required for cargo exit and recycling from
221 endosomes[31,32]. BIN1 overexpression has been linked to aging and neurodegeneration in the
222 brain[33-35] and has been seen to produce endosomal expansion and traffic jams[24,31,32].
223 Furthermore, BIN1 expression levels are known to affect ion channel trafficking in both neurons[36]
224 and ventricular myocytes[25,26]. We thus examined BIN1 expression and localization in young and
225 old myocytes and found an age-associated upregulation (Fig. 5a-b) and redistribution of BIN1
226 with old myocytes exhibiting a vesicular, endosomal pattern of BIN1-staining alongside the
227 expected t-tubule population (Fig. 5c; *left*).
228
229 ***BIN1 knockdown in old animals rejuvenates RyR2 plasticity and β-AR responsiveness***
230 Since BIN1 became upregulated and mislocalized with aging with a more endosome-like pattern
231 of expression, we hypothesized that knocking down BIN1 to young levels might resolve the
232 endosomal traffic jams and restore β-AR responsivity to aging hearts. To test this, we transduced

233 live mice with AAV9-GFP-mBIN1-shRNA (shRNA-mBIN1) or AAV9-GFP-scramble-shRNA
234 (shRNA-scrmb; control) via retro-orbital injection. Two weeks post-injection, hearts were
235 harvested, and successful shRNA-mediated knockdown of BIN1 was confirmed via both
236 immunostaining and western blot analysis. BIN1 knockdown restored youthful localization of BIN1
237 to the t-tubules (Fig. 5c; *right*), and reduced BIN1 expression levels in old hearts to young heart
238 levels (Fig. 5d-e). Control shRNA-scrmb transduced old hearts had similar BIN1 expression levels
239 to non-transduced old hearts (Fig. 5d-e) and in all experiments, cells isolated from shRNA-scrmb
240 transduced hearts maintained an old phenotype (Fig. 5c, 5f-m, Supplementary Fig. 3, and
241 Supplementary Table 1). Contrary to our hypothesis, I_{Ca} recordings from shRNA-mBIN1
242 transduced old myocytes did not indicate restoration of ISO responsivity (Fig. 5f-g, Supplementary
243 Fig. 3a). In line with that finding, BIN1 knockdown did not reverse the endosomal swelling seen
244 with aging suggesting that it is not an essential contributor to endosomal dysfunction in
245 cardiomyocytes (Supplementary Fig. 4). However, basal Ca^{2+} transient amplitude in shRNA-
246 mBIN1 transduced old myocytes resembled that of young myocytes and *β*-adrenergic
247 responsiveness was fully restored to young levels (Fig. 5h-i, Supplementary Fig. 3b).
248 The recovery of Ca^{2+} transient amplitude suggested that BIN1 knockdown may
249 predominantly impact RyR2 function and/or distribution and not $Ca_V1.2$. To investigate that
250 possibility, we performed SMLM on shRNA-mBIN1 transduced myocytes finding the nanoscale
251 distribution of $Ca_V1.2$ was unaltered compared to non-transduced old myocytes in that they
252 remained basally super-clustered and did not recover the super-clustering response to ISO (Fig.
253 5j-k, and Supplementary Fig. 3c). In contrast, RyR2 appeared rejuvenated and exhibited a young
254 cell-like nanoscale distribution and response to ISO (Fig. 5l-m, and Supplementary Fig. 3d).
255 Overall, these results suggest that knockdown of BIN1 in aging hearts recovers cardiac *β*-
256 adrenergic responsiveness by restoring RyR2 clustering plasticity.
257
258 ***BIN1 knockdown in old animals rescues systolic but not diastolic function***

259 Since all our experiments were performed in isolated cells, the question remained, would
260 BIN1 knockdown improve old heart contractile function *in vivo*? To address this, we performed
261 echocardiography in young, old, and old shRNA-transduced mice. In conscious mice fractional
262 shortening (FS) and ejection fractions (EF) were reduced in old mice compared to young (Fig. 6a-
263 c) suggesting an age-dependent systolic dysfunction. To examine the effects of shRNA-scrmb or
264 shRNA-mBIN1 on old heart function, we performed echocardiograms on old mice to record their
265 initial function prior to treatment with shRNA (Fig. 6d-e; *left*). Those mice were then retro-orbitally
266 injected with either shRNA-scrmb (control) or shRNA-mBIN1 and after a two-week transduction
267 period, repeat echocardiograms were obtained (Fig. 6d-e; *right*). In agreement with the
268 rejuvenating effects of BIN1 knockdown observed in the *in vitro* functional analysis of Ca^{2+}
269 transients, basal ventricular function was restored to a more youthful phenotype upon BIN1
270 knockdown, with shRNA-mBIN1 treated old mice displaying improved FS and EF (Fig. 6f-g).
271 Old mice also exhibited signs of left ventricular (LV) hypertrophy including increased LV
272 mass (Supplementary Fig. 5a). Two weeks of BIN1 knockdown did not significantly improve LV
273 mass although there was a downward trajectory toward a more youthful LV mass in paired old
274 mice pre- and post-shRNA-mBIN1 that was not apparent in the shRNA-scrmb cohort
275 (Supplementary Fig. 5b). LV end diastolic volumes (EDV) and end systolic volumes (ESV) were
276 significantly increased in old mice compared to young (Supplementary Fig. 5e and g). The
277 resultant increase in preload in old mice would be expected to enhance ventricular output via the
278 Frank-Starling mechanism to maintain stroke volume in the face of reduced contractility. shRNA-
279 mBIN1 transduction in old mice significantly reduced EDV and ESV to youthful levels
280 (Supplementary Fig. 5f and h). Accordingly, cardiac output (CO) was significantly rejuvenated by
281 BIN1 knockdown in old mice, increasing from a mean of 14.82 mL/min pre-injection to 17.32
282 mL/min two weeks post-knockdown and approaching the 18.61 mL/min seen in young mice
283 (Supplementary Fig. 5i-j). The restoration of youthful CO, EDV, ESV, FS and EF by BIN1
284 knockdown suggests this treatment rejuvenates systolic function in old mice.

285 We further measured the *in vivo* effects of ISO on ventricular contractile function by
286 performing echocardiograms on anesthetized young and old mice before and after intraperitoneal
287 injection of ISO. As above, repeat echocardiograms were performed on old mice 2-weeks after
288 retro-orbital injection of shRNA-scrmb or shRNA-mBIN1 (Supplementary Figs. 6 and 7). As has
289 been previously reported, resting and ISO-stimulated heart rates were significantly lower in old
290 mice compared to young[37], but neither the scrambled shRNA nor the BIN1 knockdown had any
291 significant effect on heart rate suggesting that pacemaker activity is not affected by these
292 treatments (Supplementary Figs. 5c-d, 6a-b, and 7a-b). In agreement with the *in vivo* data from
293 conscious mice, basal ventricular contractile function was rejuvenated by BIN1 knockdown with
294 CO, FS, EF, EDV and ESV (Supplementary Figs. 6 and 7) all improving toward youthful levels.
295 Importantly this effect was not observed in shRNA-scrmb transduced mice suggesting a specific
296 effect of BIN1 knockdown.
297 To assess changes in diastolic function with aging, we performed pulsed wave Doppler
298 imaging on unconscious mice. Old mice displayed an enhanced isovolumetric relaxation time
299 (IVRT) and reduced mitral valve early to late ventricular filling velocity ratio (MV E/A), indicative
300 of diastolic dysfunction, which was not remedied with BIN1 knockdown (Fig. 7). Altogether, these
301 results suggest that BIN1 knockdown may represent a new therapeutic strategy to improve age-
302 related deficits in systolic function.
303
304 ***Age-dependent decrease in myofilament Ca^{2+} sensitivity is rescued by BIN1 knockdown***
305 Ca^{2+} sensitivity of the myofilaments can also influence systolic and diastolic function thus we
306 examined the expression and phosphorylation state of two cardiac myofilament proteins that are
307 known to impact Ca^{2+} sensitivity in a phosphorylation-dependent manner, specifically cardiac
308 troponin-I (cTnI)[38,39] and cardiac myosin binding protein-C (cMyBP-C)[40,41]. We probed for these
309 myofilament proteins in heart lysates isolated from each cohort. We began with cTnI finding its
310 total expression increased with aging, but relative expression of the phosphorylated form

311 (pS23/24) reduced (Fig. 8a-c). While shRNA-mBIN1 treatment displayed a trend toward a more
312 youthful pS23/24 expression, the trend did not become significant. Total expression of cMyBP-C
313 was unaltered with aging but its phosphorylation at S273 was significantly decreased (Fig. 8d-f).
314 shRNA-mBIN1 treatment restored youthful cMyBP-C pS273 expression levels. Our results
315 support a model where reduced phosphorylation of cMyBP-C in old hearts contributes to deficits
316 in contractile function while reduced cTnI phosphorylation favors longer relaxation and diastolic
317 dysfunction. BIN1 knockdown appears to restore systolic but not diastolic function by improving
318 phosphorylation of cMyBP-C but not cTnI.
319

320 **Discussion**

321 We report six novel findings that provide insight into the mechanistic basis of age-related cardiac
322 dysfunction and reveal BIN1 as a new therapeutic target to rejuvenate the aging heart and extend
323 cardiovascular health into old age: 1) patch clamp and Ca^{2+} transient recordings revealed an age-
324 associated loss of cardiac *β*-adrenergic responsiveness measured by the functional augmentation
325 of $Ca_V1.2$ and RyR2 channel activity; 2) super-resolution imaging and PLA revealed an age-
326 associated dysregulation of $Ca_V1.2$ and RyR2 clustering plasticity, and juxta-positioning at dyads;
327 3) examination of endosomal pools and $Ca_V1.2$ dynamics revealed ISO-stimulated Ca^{2+} channel
328 mobility and recycling is impaired in aging due to trafficking deficits that cause endosomal traffic
329 jams; 4) western blots and super-resolution imaging revealed that BIN1, important for t-tubule
330 biogenesis[27], and $Ca_V1.2$, RyR2[18,25,26] and sarcomere[42] organization, is overexpressed in aging
331 hearts; 5) shRNA-mediated BIN1 knockdown to youthful levels rejuvenated RyR2 clustering
332 plasticity, basal Ca^{2+} transient amplitudes and their functional augmentation by *β*-AR-stimulation,
333 and myofilament protein phosphorylation; and finally 6) *in vivo* echocardiography and Doppler
334 imaging demonstrated that BIN1 knockdown in old mice restored youthful systolic (but not
335 diastolic) function and substantially reversed the aging phenotype. Our knockdown approach
336 using AAV9 packaged shRNA against BIN1 is rapid, occurring within 2 weeks of retro-orbital
337 injection, and has translational potential as AAVs are approved for use in humans[43].

338 Prior studies have shown that basal $Ca_V1.2$ activity and *β*-AR-mediated I_{Ca} enhancement
339 are altered with aging[44]. However, the effects on basal $Ca_V1.2$ currents appear to vary depending
340 on sex, species, and possibly even strain with various groups reporting enhanced[44-46],
341 unchanged[47], or reduced[48-50] currents in aged models. In our hands, myocytes from 24-month-old
342 C57BL/6J mice had enhanced basal $Ca_V1.2$ currents compared to young (3-month-old). Old
343 myocytes also exhibited basally enhanced Ca^{2+} transient amplitudes. Prior findings on Ca^{2+}
344 transient alterations in the aging myocardium range from basal amplitude augmentation[45,51] and

345 faster decay kinetics[52] to no or little reported change[50], to basal reduction in CaT amplitude and
346 slower rate of decay[46,53]. This echoes the variability in age-associated alterations of I_{Ca} and
347 reflects the complexity of aging. Importantly though, and in line with our results, there is agreement
348 that the ability of *β*-AR-signaling to augment Ca^{2+} transient amplitude and tune EC-coupling and
349 inotropy is diminished with aging[7,8,54-59].

350 This study provides the first evidence linking age-associated *β*-AR hypo-responsivity to
351 alterations in Ca^{2+} channel clustering and organization. Super-resolution microscopy studies of
352 the nanoscale arrangement of $Ca_V1.2$ and RyR2 have fueled the emerging concept that tunable
353 insertion, recycling, and clustering of these channels physiologically during receptor signaling
354 cascades or pathologically in disease, affects Ca^{2+} release efficiency and myocardial
355 contractility[15,16,19,20,60-62]. Larger $Ca_V1.2$ clusters facilitate enhanced $Ca_V1.2$-$Ca_V1.2$ physical
356 interactions and cooperative gating that amplifies I_{Ca}[16,17,63] while larger RyR2 clusters favor
357 enhanced Ca^{2+} spark frequency and larger Ca^{2+} transients[21]. We previously reported that acute
358 *β*-AR activation in young ventricular myocytes promotes rapid, dynamic augmentation of
359 sarcolemmal $Ca_V1.2$ channel abundance as channels are mobilized from endosomal reservoirs
360 via fast and slow recycling pathways[15,16]. Here, super-resolution microscopy and dynamic channel
361 tracking experiments demonstrated that this response is impaired with aging, such that $Ca_V1.2$
362 are basally super-clustered to a similar extent to that seen in young ISO-stimulated myocytes.
363 These results, correlated with the basally elevated I_{Ca} and impaired current augmentation with
364 ISO, hint that the endosomal reservoir of $Ca_V1.2$ cargo has already been expended and/or
365 endosomal recycling pathways are impaired. Our data suggest the latter is true, revealing reduced
366 ISO-induced insertions in old myocytes, an aggregation of channels on swollen endosomes, and
367 a larger pool of static channels that appear stranded in the sarcolemma. Whether this pool of
368 static channels reflects increased lifetime of $Ca_V1.2$ in the membrane remains to be established.
369 The main conclusion from this data is that the endosomal pathway and homeostatic regulation of
370 $Ca_V1.2$ channel expression at the sarcolemma is impaired with aging.

371 Deficiencies in recycling and endosomal enlargement are familiar sights in Alzheimer's
372 disease (AD) where endosomal enlargement is the first neuro-cytopathological hallmark of AD,
373 visible even before neurofibrillary tangles or amyloid β plaques[23]. An imbalance in cargo trafficking
374 into and out of endosomes is thought to result in endosome swelling and recycling pathway
375 deficiencies termed endosomal traffic jams[24]. As mentioned earlier, alterations in BIN1 expression
376 are thought to contribute to endosomal dysregulation in AD neurons. Thus, when we found BIN1
377 expression was significantly increased in aging, and appeared to assume a more endosomal
378 localization pattern, we thought, since it was in the "right place at the right time" that knockdown
379 of BIN1 would restore youthful endosomal trafficking and improve $Ca_V1.2$ channel cargo
380 mobilization, recovering *β*-AR responsivity and $Ca_V1.2$ channel functional augmentation. That
381 hypothesis was thoroughly disproven with results showing BIN1 knockdown did not in fact
382 accomplish any of those things. Several other proteins have been implicated as sources or
383 contributors to endosomal dysfunction and swelling in AD neurons as reviewed[24]. Future studies
384 should investigate whether any of those proteins underlie age-associated endosomal dysfunction
385 and impaired $Ca_V1.2$ recycling in ventricular myocytes.

386 On the other side of the dyadic cleft, RyR2 also display enlarged basal clusters that fail to
387 undergo augmentation with ISO in aging myocytes. Other groups have reported phosphorylation-
388 stimulated clustering of RyR2[18,19] but this is the first report of disruption of this dynamic response
389 with aging. Furthermore, it is the first to find that spatial proximity between $Ca_V1.2$ and RyR2
390 increases with acute ISO in young myocytes. This suggests rapid dynamic formation of new dyads
391 or expansion of existing dyads during ISO-stimulation. The implication here is that *β*-AR activation
392 stimulates parallel $Ca_V1.2$ and RyR2 cluster expansion on either side of the dyadic cleft to
393 maximize the efficiency of Ca^{2+} release but that this additional tuning capacity or reserve is lost
394 with aging and is apparently already expended at rest. Cardiac RyR2 trafficking and mobility is
395 poorly understood and understudied but one report has linked RyR2 redistribution upon
396 phosphorylation to BIN1, evidenced by reduced recruitment of phosphorylated RyR2 to dyadic

397 regions in cardiac-specific *BIN1* knockout cardiomyocytes[18]. Interestingly, BIN1 knockdown in old
398 mice had a more profound effect on RyR2 distribution, Ca^{2+} transient amplitude, and inotropy than
399 it had on $Ca_V1.2$. To that end, RyR2 nanoscale distribution was rejuvenated by BIN1 knockdown
400 in old hearts but $Ca_V1.2$ still exhibited the old super-clustered phenotype and heightened basal
401 I_{Ca}. So, while our initial rationale for knocking down BIN1 in the aging heart BIN1 was flawed,
402 serendipitously we discovered that BIN1 knockdown has a rejuvenating effect on RyR2.

403 Echocardiography confirmed the benefits of BIN1 knockdown on the aging heart with
404 parameters of systolic function including EF, FS, and CO all substantially improved after just a
405 two-week knockdown of BIN1. EDV and ESV also declined to youthful levels reflecting the
406 increased contractile function. In humans, resting systolic function is generally preserved with
407 aging, however it becomes significantly impaired during exercise and acute stress[3,64,65]. The
408 resting systolic dysfunction observed in the current study may reflect the difference between
409 human and mouse heart's basal autonomic balance at room temperature. Mice have relatively
410 more sympathetic nervous system activity at rest than humans. With aging, autonomic balance
411 becomes even more tilted toward sympathetic activity as parasympathetic input appears
412 reduced[66,67]. In this way, a resting mouse heart is not necessarily a fair comparison to a resting
413 human heart and may instead be a better reflection of an exercising human heart. Thus, BIN1
414 knockdown may present a therapeutic option to enhance systolic function in aging humans during
415 acute exercise and stress.

416 Diastolic dysfunction is a more universal finding with aging in both humans and mice[4,68]
417 and our findings of a prolonged IVRT with aging and reduced E/A ratio agree with prior studies
418 reporting impaired relaxation. However, BIN1 knockdown did not remedy diastolic dysfunction.
419 This is perhaps expected as enhanced fibrosis[68] with aging is one of the main causes of the
420 enhanced stiffness that underlies diastolic issues in the aging heart, and there is no reason to
421 suspect that BIN1 knockdown would improve fibrosis.

422 Reduced Ca^{2+} sensitivity of the myofilaments can also contribute to diastolic dysfunction.
423 Enhanced phosphorylation of the thin myofilament protein cTnI by PKA at ser-23 and -24
424 accelerates myocardial relaxation by reducing myofilament Ca^{2+} sensitivity, favoring Ca^{2+}
425 dissociation from troponin-C, and leading to faster actin-myosin detachment[38,39]. Our results
426 indicate that aging hearts display significantly lower levels of cTnI phosphorylation favoring slower
427 relaxation. This deficit was not improved or corrected by BIN1 knockdown and diastolic
428 dysfunction prevailed. Given the reciprocal relationship between cTnI phosphorylation and
429 myofilament Ca^{2+} sensitivity, one would predict that the age-associated reduction in cTnI pS23/24
430 levels would result in increased Ca^{2+} sensitivity in old mice compared to young, leading to
431 increased Ca^{2+}-dependent force generation. However, our *in vitro* finding of larger amplitude Ca^{2+}
432 transients in old myocytes accompanied by reduced *in vivo* contractile function in old mice
433 suggests quite the opposite. Specifically, our functional results suggest an age-associated
434 reduction in the Ca^{2+} sensitivity of the myofilaments that is remedied by BIN1 knockdown. Thus,
435 we broadened our search to examine cMyBP-C, another myofilament protein. Decreased
436 phosphorylation of cMyBP-C causes decreases myofilament Ca^{2+} sensitivity[41] and contractile
437 dysfunction in heart failure patients[40]. Furthermore, in the dephosphorylated state, cMyBP-c
438 inhibits actin-myosin interactions leading to reduced force development[41]. We found old mouse
439 hearts had lower cMyBP-C pS273[69] expression levels than young hearts. A similar age-
440 associated decline in cMyBP-C phosphorylation has been reported by others and found to
441 correlate with deterioration of cardiac function[70]. Furthermore, phosphorylation-mimetic cMyBP-
442 C mutant mice exhibit preserved cardiac function and enhanced longevity suggesting
443 phosphorylation of cMyBP-C is cardioprotective[70]. In a novel finding, we report that BIN1
444 knockdown rescues cMyBP-C pS273 phosphorylation levels which potentially explains the
445 improved contractile function and Ca^{2+} sensitivity in shRNA-mBIN1 transduced mice. But how can
446 one link BIN1 expression levels to sarcomeric proteins? While we do not yet have the full
447 mechanistic picture of how this occurs, there is evidence that BIN1 binds to and influences

448 sarcomeric proteins. For example, in skeletal muscle, BIN1 is said to act as an essential adaptor
449 protein and scaffold that promotes mature sarcomere assembly[42]. Increased BIN1 expression is
450 also known to promote enhanced expression of myosin heavy chain[71] and to associate with and
451 stabilize actin filaments[72]. Future studies should examine the mechanism of BIN1 regulatory
452 influences over cMyBP-C but it is an intriguing idea first proposed by Fernando et al in 2009[42],
453 that a single protein (BIN1) could orchestrate sarcolemmal and sarcomeric architecture and
454 regulation.

455 It is important to mention that although our study focused on the effects of BIN1
456 upregulation with aging, prior work has revealed that BIN1 *downregulation* is associated with heart
457 failure[26,29] and that exogenous supplementation of a cardiac specific isoform of BIN1 can improve
458 cardiac function in mice with pressure overload-induced heart failure[73]. It is possible that BIN1
459 levels must be tightly regulated and that any deviation from a homeostatic normal level could be
460 damaging. In Alzheimer's disease such a model has been presented where too much or too little
461 BIN1 expression are both associated with enhanced risk of disease[35,74].

462 In summary, we find that BIN1 knockdown restores youthful Ca^{2+} transient amplitude, *β*-
463 AR mediated transient augmentation, and *in vivo* systolic function in the aging myocardium. This
464 study sets the groundwork for future work and raises the hope that a similar approach could
465 improve cardiac function, restore exercise tolerance, and increase capacity to endure acute stress
466 in elderly patients.
467

468 **Acknowledgments**

469 We extend our thanks to Dr. Sakthivel Sadayappan for the generous gift of the total cMyBP-C
470 antibody and the cMyBP-C Ser-273 phospho-site specific antibody[69]. We thank Dr. L. Fernando
471 Santana and Heather Spooner for reading and providing critical suggestions on our manuscript.

472

473 **Sources of Funding**

474 This work was supported by NIH R01AG063796 and R01HL159304 to R.E.D.; R01GM127513
475 and RF1NS131379 to E.J.D.; by the NIGMS funded Pharmacology Training Program T32
476 GM099608 and later by an AHA Predoctoral Fellowship 827909 to T.L.V., by a Postdoctoral
477 Fellowship from NIH T32 Training Grant in Basic & Translational Cardiovascular Science T32
478 HL086350 and NIH F32 HL149288 to P.N.T.; and by NIH R01HL085727, R01HL085844,
479 R01HL137228, S10OD010389 Core Equipment Grant, and VA Merit Review Grant I01 BX000576
480 and I01 CX001490 to N.C. Graphical Abstract was generated using Biorender.com.

481

482 **Disclosures**

483 None.

484

485

References

1 Roth, G. A. *et al.* Global Burden of Cardiovascular Diseases and Risk Factors, 1990-2019: Update From the GBD 2019 Study. *Journal of the American College of Cardiology* **76**, 2982-3021, doi:10.1016/j.jacc.2020.11.010 (2020).

2 Dhingra, R. & Vasan, R. S. Age as a risk factor. *Med Clin North Am* **96**, 87-91, doi:10.1016/j.mcna.2011.11.003 (2012).

3 Dai, D. F., Chen, T., Johnson, S. C., Szeto, H. & Rabinovitch, P. S. Cardiac aging: from molecular mechanisms to significance in human health and disease. *Antioxid Redox Signal* **16**, 1492-1526, doi:10.1089/ars.2011.4179 (2012).

4 Strait, J. B. & Lakatta, E. G. Aging-Associated Cardiovascular Changes and Their Relationship to Heart Failure. *Heart Failure Clinics* **8**, 143-164, doi:10.1016/j.hfc.2011.08.011 (2012).

5 Lakatta, E. G. & Sollott, S. J. Perspectives on mammalian cardiovascular aging: humans to molecules. *Comp Biochem Physiol A Mol Integr Physiol* **132**, 699-721 (2002).

6 Ferrara, N. *et al.* beta-adrenergic receptor responsiveness in aging heart and clinical implications. *Front Physiol* **4**, 396, doi:10.3389/fphys.2013.00396 (2014).

7 Xiao, R. P. *et al.* Age-associated reductions in cardiac beta1- and beta2-adrenergic responses without changes in inhibitory G proteins or receptor kinases. *J Clin Invest* **101**, 1273-1282 (1998).

8 Xiao, R. P., Spurgeon, H. A., O'Connor, F. & Lakatta, E. G. Age-associated changes in beta-adrenergic modulation on rat cardiac excitation-contraction coupling. *J Clin Invest* **94**, 2051-2059 (1994).

9 Osterrieder, W. *et al.* Injection of subunits of cyclic AMP-dependent protein kinase into cardiac myocytes modulates Ca2+ current. *Nature* **298**, 576-578 (1982).

10 Hartzell, H. C., Mery, P. F., Fischmeister, R. & Szabo, G. Sympathetic regulation of cardiac calcium current is due exclusively to cAMP-dependent phosphorylation. *Nature* **351**, 573-576, doi:10.1038/351573a0 (1991).

11 Liu, G. *et al.* Mechanism of adrenergic CaV1.2 stimulation revealed by proximity proteomics. *Nature* **577**, 695-700, doi:10.1038/s41586-020-1947-z (2020).

12 Manning, J. R. *et al.* Rad GTPase deletion increases L-type calcium channel current leading to increased cardiac contraction. *J Am Heart Assoc* **2**, e000459, doi:10.1161/JAHA.113.000459 (2013).

13 Yue, D. T., Herzig, S. & Marban, E. Beta-adrenergic stimulation of calcium channels occurs by potentiation of high-activity gating modes. *Proc Natl Acad Sci U S A* **87**, 753-757. (1990).

14 Bean, B. P., Nowycky, M. C. & Tsien, R. W. Beta-adrenergic modulation of calcium channels in frog ventricular heart cells. *Nature* **307**, 371-375 (1984).

15 Del Villar, S. G. *et al.* beta-Adrenergic control of sarcolemmal CaV1.2 abundance by small GTPase Rab proteins. *Proc Natl Acad Sci U S A* **118**, doi:10.1073/pnas.2017937118 (2021).

16 Ito, D. W. *et al.* beta-adrenergic-mediated dynamic augmentation of sarcolemmal CaV 1.2 clustering and co-operativity in ventricular myocytes. *J Physiol* **597**, 2139-2162, doi:10.1113/JP277283 (2019).

527 17 Dixon, R. E., Navedo, M. F., Binder, M. D. & Santana, L. F. Mechanisms and Physiological
528 Implications of Cooperative Gating of Ion Channels Clusters. *Physiological reviews*,
529 doi:10.1152/physrev.00022.2021 (2021).

530 18 Fu, Y. *et al.* Isoproterenol Promotes Rapid Ryanodine Receptor Movement to Bridging
531 Integrator 1 (BIN1)-Organized Dyads. *Circulation* **133**, 388-397,
532 doi:10.1161/CIRCULATIONAHA.115.018535 (2016).

533 19 Asghari, P. *et al.* Cardiac ryanodine receptor distribution is dynamic and changed by auxiliary
534 proteins and post-translational modification. *Elife* **9**, doi:10.7554/eLife.51602 (2020).

535 20 Dixon, R. E. Nanoscale Organization, Regulation, and Dynamic Reorganization of Cardiac
536 Calcium Channels. *Front Physiol* **12**, 810408, doi:10.3389/fphys.2021.810408 (2021).

537 21 Galice, S., Xie, Y., Yang, Y., Sato, D. & Bers, D. M. Size Matters: Ryanodine Receptor Cluster
538 Size Affects Arrhythmogenic Sarcoplasmic Reticulum Calcium Release. *J Am Heart Assoc* **7**,
539 doi:10.1161/JAHA.118.008724 (2018).

540 22 Fredriksson, S. *et al.* Protein detection using proximity-dependent DNA ligation assays.
541 *Nature biotechnology* **20**, 473-477, doi:10.1038/nbt0502-473 (2002).

542 23 Cataldo, A. M. *et al.* Endocytic pathway abnormalities precede amyloid beta deposition in
543 sporadic Alzheimer's disease and Down syndrome: differential effects of APOE genotype and
544 presenilin mutations. *Am J Pathol* **157**, 277-286, doi:10.1016/s0002-9440(10)64538-5 (2000).

545 24 Small, S. A., Simoes-Spassov, S., Mayeux, R. & Petsko, G. A. Endosomal Traffic Jams
546 Represent a Pathogenic Hub and Therapeutic Target in Alzheimer's Disease. *Trends*
547 *Neurosci* **40**, 592-602, doi:10.1016/j.tins.2017.08.003 (2017).

548 25 Hong, T. T. *et al.* BIN1 localizes the L-type calcium channel to cardiac T-tubules. *PLoS Biol*
549 **8**, e1000312, doi:10.1371/journal.pbio.1000312 (2010).

550 26 Hong, T. T. *et al.* BIN1 is reduced and Cav1.2 trafficking is impaired in human failing
551 cardiomyocytes. *Heart Rhythm* **9**, 812-820, doi:10.1016/j.hrthm.2011.11.055 (2012).

552 27 Lee, E. *et al.* Amphiphysin 2 (Bin1) and T-tubule biogenesis in muscle. *Science* **297**, 1193-
553 1196, doi:10.1126/science.1071362 (2002).

554 28 Hong, T. *et al.* Cardiac BIN1 folds T-tubule membrane, controlling ion flux and limiting
555 arrhythmia. *Nature medicine* **20**, 624-632, doi:10.1038/nm.3543 (2014).

556 29 Caldwell, J. L. *et al.* Dependence of Cardiac Transverse Tubules on the BAR Domain Protein
557 Amphiphysin II (BIN-1). *Circulation Research* **115**, 986-996,
558 doi:10.1161/circresaha.116.303448 (2014).

559 30 De La Mata, A. *et al.* BIN1 Induces the Formation of T-Tubules and Adult-Like Ca(2+) Release
560 Units in Developing Cardiomyocytes. *Stem cells (Dayton, Ohio)* **37**, 54-64,
561 doi:10.1002/stem.2927 (2019).

562 31 Pant, S. *et al.* AMPH-1/Amphiphysin/Bin1 functions with RME-1/Ehd1 in endocytic recycling.
563 *Nat Cell Biol* **11**, 1399-1410, doi:10.1038/ncb1986 (2009).

564 32 Lambert, E. *et al.* The Alzheimer susceptibility gene BIN1 induces isoform-dependent
565 neurotoxicity through early endosome defects. *Acta Neuropathol Commun* **10**, 4,
566 doi:10.1186/s40478-021-01285-5 (2022).

33 Tan, M. S., Yu, J. T. & Tan, L. Bridging integrator 1 (BIN1): form, function, and Alzheimer's disease. *Trends in molecular medicine* **19**, 594-603, doi:10.1016/j.molmed.2013.06.004 (2013).

34 Wang, H. F. *et al.* Bridging Integrator 1 (BIN1) Genotypes Mediate Alzheimer's Disease Risk by Altering Neuronal Degeneration. *J Alzheimers Dis* **52**, 179-190, doi:10.3233/JAD-150972 (2016).

35 Chapuis, J. *et al.* Increased expression of BIN1 mediates Alzheimer genetic risk by modulating tau pathology. *Mol Psychiatry* **18**, 1225-1234, doi:10.1038/mp.2013.1 (2013).

36 Schurmann, B. *et al.* A novel role for the late-onset Alzheimer's disease (LOAD)-associated protein Bin1 in regulating postsynaptic trafficking and glutamatergic signaling. *Mol Psychiatry* **25**, 2000-2016, doi:10.1038/s41380-019-0407-3 (2020).

37 Choi, S., Baudot, M., Vivas, O. & Moreno, C. M. Slowing down as we age: aging of the cardiac pacemaker's neural control. *Geroscience*, doi:10.1007/s11357-021-00420-3 (2021).

38 Pi, Y., Zhang, D., Kemnitz, K. R., Wang, H. & Walker, J. W. Protein kinase C and A sites on troponin I regulate myofilament Ca2+ sensitivity and ATPase activity in the mouse myocardium. *J Physiol* **552**, 845-857, doi:10.1113/jphysiol.2003.045260 (2003).

39 Kentish, J. C. *et al.* Phosphorylation of troponin I by protein kinase A accelerates relaxation and crossbridge cycle kinetics in mouse ventricular muscle. *Circ Res* **88**, 1059-1065, doi:10.1161/hh1001.091640 (2001).

40 El-Armouche, A. *et al.* Decreased phosphorylation levels of cardiac myosin-binding protein-C in human and experimental heart failure. *J Mol Cell Cardiol* **43**, 223-229, doi:10.1016/j.yjmcc.2007.05.003 (2007).

41 Kumar, M., Haghighi, K., Kranias, E. G. & Sadayappan, S. Phosphorylation of cardiac myosin-binding protein-C contributes to calcium homeostasis. *J Biol Chem* **295**, 11275-11291, doi:10.1074/jbc.RA120.013296 (2020).

42 Fernando, P. *et al.* Bin1 SRC homology 3 domain acts as a scaffold for myofiber sarcomere assembly. *J Biol Chem* **284**, 27674-27686, doi:10.1074/jbc.M109.029538 (2009).

43 High, K. A. & Aubourg, P. rAAV Human Trial Experience. *Adeno-Associated Virus: Methods and Protocols* **807**, 429-457, doi:10.1007/978-1-61779-370-7_18 (2011).

44 Josephson, I. R., Guia, A., Stern, M. D. & Lakatta, E. G. Alterations in properties of L-type Ca channels in aging rat heart. *J Mol Cell Cardiol* **34**, 297-308, doi:10.1006/jmcc.2001.1512 (2002).

45 Dibb, K. M., Rueckschloss, U., Eisner, D. A., Isenberg, G. & Trafford, A. W. Mechanisms underlying enhanced cardiac excitation contraction coupling observed in the senescent sheep myocardium. *J Mol Cell Cardiol* **37**, 1171-1181, doi:10.1016/j.yjmcc.2004.09.005 (2004).

46 Isenberg, G., Borschke, B. & Rueckschloss, U. Ca2+ transients of cardiomyocytes from senescent mice peak late and decay slowly. *Cell Calcium* **34**, 271-280, doi:10.1016/s0143-4160(03)00121-0 (2003).

47 Walker, K. E., Lakatta, E. G. & Houser, S. R. Age associated changes in membrane currents in rat ventricular myocytes. *Cardiovascular research* **27**, 1968-1977, doi:10.1093/cvr/27.11.1968 (1993).

608 48 Grandy, S. A. & Howlett, S. E. Cardiac excitation-contraction coupling is altered in myocytes
609 from aged male mice but not in cells from aged female mice. *Am J Physiol Heart Circ Physiol*
610 **291**, H2362-2370, doi:10.1152/ajpheart.00070.2006 (2006).

611 49 Liu, S. J., Wyeth, R. P., Melchert, R. B. & Kennedy, R. H. Aging-associated changes in whole
612 cell K(+) and L-type Ca(2+) currents in rat ventricular myocytes. *Am J Physiol Heart Circ*
613 *Physiol* **279**, H889-900, doi:10.1152/ajpheart.2000.279.3.H889 (2000).

614 50 Kong, C. H. T. *et al.* The Effects of Aging on the Regulation of T-Tubular ICa by Caveolin in
615 Mouse Ventricular Myocytes. *J Gerontol A Biol Sci Med Sci* **73**, 711-719,
616 doi:10.1093/gerona/glx242 (2018).

617 51 Rueckschloss, U., Villmow, M. & Klockner, U. NADPH oxidase-derived superoxide impairs
618 calcium transients and contraction in aged murine ventricular myocytes. *Exp Gerontol* **45**,
619 788-796, doi:10.1016/j.exger.2010.05.002 (2010).

620 52 Francis Stuart, S. D. *et al.* Age-related changes in cardiac electrophysiology and calcium
621 handling in response to sympathetic nerve stimulation. *J Physiol* **596**, 3977-3991,
622 doi:10.1113/JP276396 (2018).

623 53 Janczewski, A. M., Spurgeon, H. A. & Lakatta, E. G. Action potential prolongation in cardiac
624 myocytes of old rats is an adaptation to sustain youthful intracellular Ca2+ regulation. *J Mol*
625 *Cell Cardiol* **34**, 641-648, doi:10.1006/jmcc.2002.2004 (2002).

626 54 White, M. *et al.* Age-related changes in beta-adrenergic neuroeffector systems in the human
627 heart. *Circulation* **90**, 1225-1238 (1994).

628 55 Lakatta, E. G. Deficient Neuroendocrine Regulation of the Cardiovascular-System with
629 Advancing Age in Healthy Humans. *Circulation* **87**, 631-636 (1993).

630 56 Stratton, J. R. *et al.* Differences in cardiovascular responses to isoproterenol in relation to age
631 and exercise training in healthy men. *Circulation* **86**, 504-512 (1992).

632 57 Davies, C. H., Ferrara, N. & Harding, S. E. Beta-adrenoceptor function changes with age of
633 subject in myocytes from non-failing human ventricle. *Cardiovascular research* **31**, 152-156
634 (1996).

635 58 Lakatta, E. G., Gerstenblith, G., Angell, C. S., Shock, N. W. & Weisfeldt, M. L. Diminished
636 inotropic response of aged myocardium to catecholamines. *Circ Res* **36**, 262-269 (1975).

637 59 Cerbai, E. *et al.* Beta-adrenoceptor subtypes in young and old rat ventricular myocytes: a
638 combined patch-clamp and binding study. *Br J Pharmacol* **116**, 1835-1842 (1995).

639 60 MacQuaide, N. *et al.* Ryanodine receptor cluster fragmentation and redistribution in persistent
640 atrial fibrillation enhance calcium release. *Cardiovascular research* **108**, 387-398,
641 doi:10.1093/cvr/cvv231 (2015).

642 61 Kolstad, T. R. *et al.* Ryanodine receptor dispersion disrupts Ca(2+) release in failing cardiac
643 myocytes. *Elife* **7**, doi:10.7554/eLife.39427 (2018).

644 62 Hou, Y. *et al.* Nanoscale Organisation of Ryanodine Receptors and Junctophilin-2 in the
645 Failing Human Heart. *Front Physiol* **12**, 724372, doi:10.3389/fphys.2021.724372 (2021).

646 63 Dixon, R. E., Yuan, C., Cheng, E. P., Navedo, M. F. & Santana, L. F. Ca2+ signaling
647 amplification by oligomerization of L-type Cav1.2 channels. *Proc Natl Acad Sci U S A* **109**,
648 1749-1754, doi:10.1073/pnas.1116731109 (2012).

649 64 Schulman, S. P. *et al.* Age-related decline in left ventricular filling at rest and exercise. *Am J*
650 *Physiol* **263**, H1932-1938, doi:10.1152/ajpheart.1992.263.6.H1932 (1992).

651 65 Fleg, J. L. & Lakatta, E. G. in *Cardiovascular disease in the elderly* 21-64 (CRC Press,
652 2008).

653 66 Comelli, M. *et al.* Rhythm dynamics of the aging heart: an experimental study using conscious,
654 restrained mice. *Am J Physiol Heart Circ Physiol* **319**, H893-H905,
655 doi:10.1152/ajpheart.00379.2020 (2020).

656 67 Piantoni, C. *et al.* Age-Related Changes in Cardiac Autonomic Modulation and Heart Rate
657 Variability in Mice. *Front Neurosci* **15**, 617698, doi:10.3389/fnins.2021.617698 (2021).

658 68 Dai, D. F. *et al.* Overexpression of catalase targeted to mitochondria attenuates murine
659 cardiac aging. *Circulation* **119**, 2789-2797, doi:CIRCULATIONAHA.108.822403
660 [pii]10.1161/CIRCULATIONAHA.108.822403 (2009).

661 69 Copeland, O. *et al.* Analysis of cardiac myosin binding protein-C phosphorylation in human
662 heart muscle. *J Mol Cell Cardiol* **49**, 1003-1011, doi:10.1016/j.yjmcc.2010.09.007 (2010).

663 70 Rosas, P. C. *et al.* Cardiac Myosin Binding Protein-C Phosphorylation Mitigates Age-Related
664 Cardiac Dysfunction: Hope for Better Aging? *JACC Basic Transl Sci* **4**, 817-830,
665 doi:10.1016/j.jacbts.2019.06.003 (2019).

666 71 Wechsler-Reya, R. J., Elliott, K. J. & Prendergast, G. C. A role for the putative tumor
667 suppressor Bin1 in muscle cell differentiation. *Molecular and cellular biology* **18**, 566-575,
668 doi:10.1128/MCB.18.1.566 (1998).

669 72 Drager, N. M. *et al.* Bin1 directly remodels actin dynamics through its BAR domain. *Embo*
670 *Reports* **18**, 2051-2066, doi:10.15252/embr.201744137 (2017).

671 73 Li, J., Agvanian, S., Zhou, K., Shaw, R. M. & Hong, T. Exogenous Cardiac Bridging Integrator
672 1 Benefits Mouse Hearts With Pre-existing Pressure Overload-Induced Heart Failure. *Front*
673 *Physiol* **11**, 708, doi:10.3389/fphys.2020.00708 (2020).

674 74 Calafate, S., Flavin, W., Verstreken, P. & Moechars, D. Loss of Bin1 Promotes the
675 Propagation of Tau Pathology. *Cell Rep* **17**, 931-940, doi:10.1016/j.celrep.2016.09.063
676 (2016).

677

678

679 **Figures and Figure Legends**

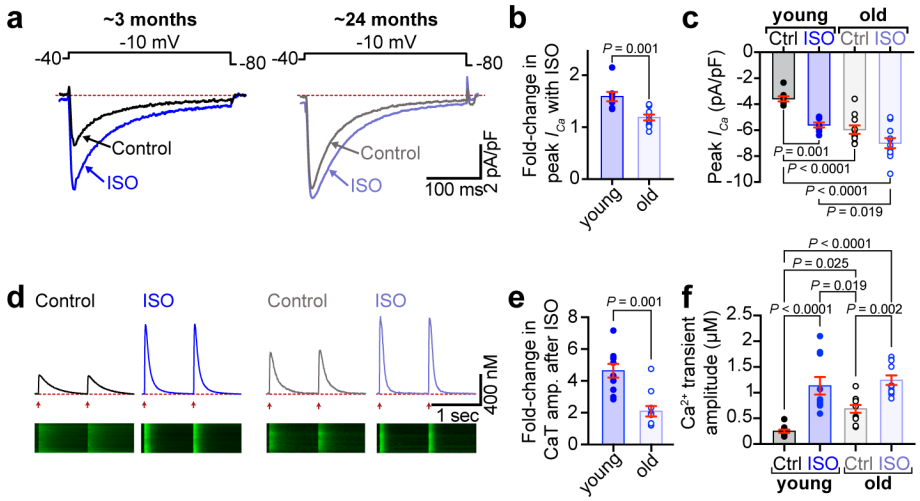

680

681 **Figure 1. *β*-AR stimulated augmentation of I_{Ca} and Ca^{2+} transients is diminished in aging.**
682 **a**, representative whole-cell currents elicited from young and old ventricular myocytes before
683 (control; black) and during application of ISO (blue). **b**, dot-plots showing the fold change in peak
684 current with ISO in young (N = 6, n = 8) and old (N = 5, n = 11) myocytes. **c**, dot-plots showing
685 peak I_{Ca} before and after ISO. **d**, representative Ca^{2+} transients recorded before and after ISO
686 from paced young (N = 6, n = 10) and old (N = 5, n = 11) myocytes. **e**, dot-plots showing the fold-
687 increase in Ca^{2+} transient amplitude after ISO and **f**, Ca^{2+} transient amplitude before and after
688 ISO. Unpaired Student's t-tests were performed on data sets displayed in b and e. Two-way
689 ANOVAs with post-hoc Tukey's multiple comparison tests were performed on data displayed in c
690 and f.

691

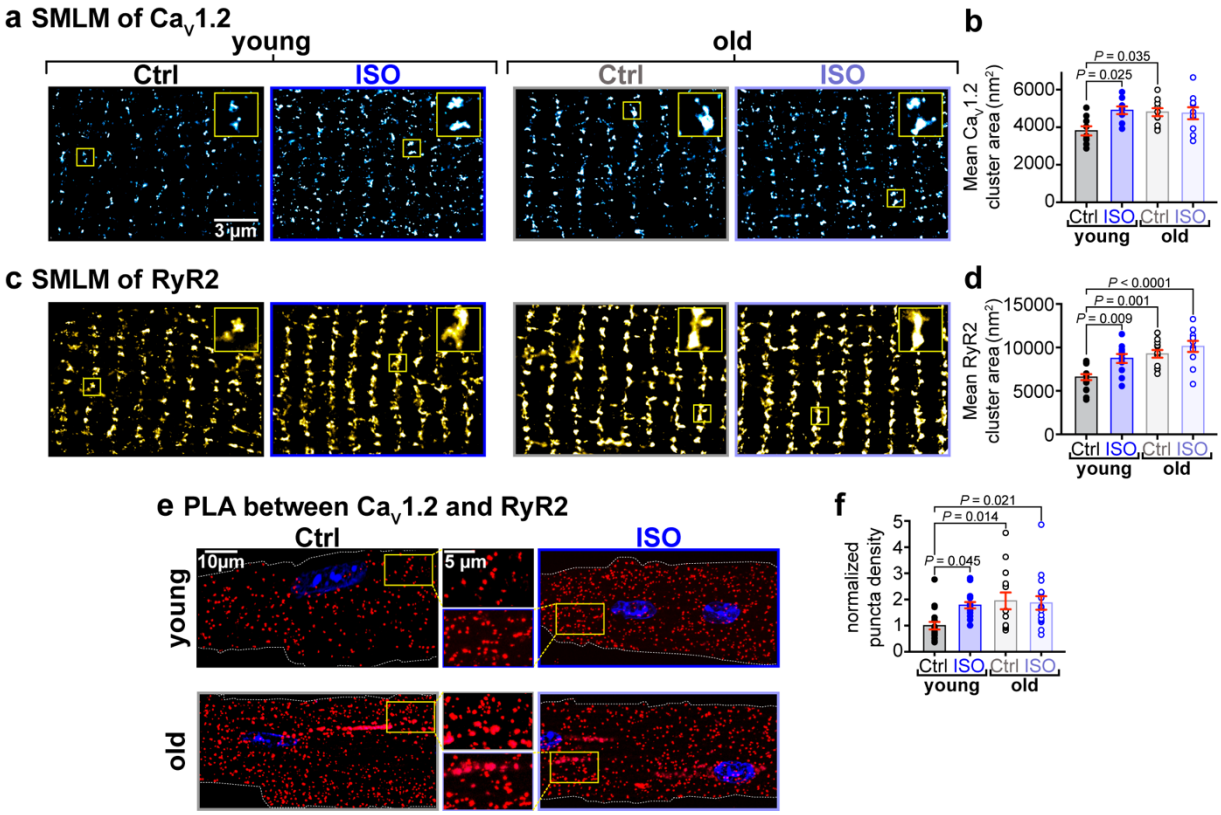

Figure 2. Basal super-clustering, impaired β-AR responsiveness, and enhanced proximity of $Ca_V1.2$ and RyR2 in aged myocytes. **a**, SMLM localization maps showing $Ca_V1.2$ channel localization and distribution in the t-tubules of young and old ventricular myocytes with or without ISO-stimulation. Yellow boxes indicate the location of the regions of interest magnified in the top right of each image. **b**, dot-plots showing mean $Ca_V1.2$ channel cluster areas in young (control: N = 3, n = 9; ISO: N = 3, n = 9) and old (control: N = 4, n = 11; ISO: N = 4, n = 10) myocytes. **c** and **d**, show the same for RyR2 in young (control: N = 3, n = 17; ISO: N = 3, n = 11) and old (control: N = 3, n = 12; ISO: N = 3, n = 11) myocytes. **e**, Representative fluorescence PLA (red)/DAPI (blue) images of myocytes with and without ISO-stimulation. **f**, dot-plot summarizing the cellular density of PLA fluorescent puncta normalized to the density in young control cells (young control: N = 3, n = 19; young ISO: N = 3, n = 16; old control: N = 3, n = 14; old ISO: N = 3, n = 16). Statistical analyses on data summarized in b, d, and f were performed using two-way ANOVAs with post-hoc Tukey's multiple comparison tests.

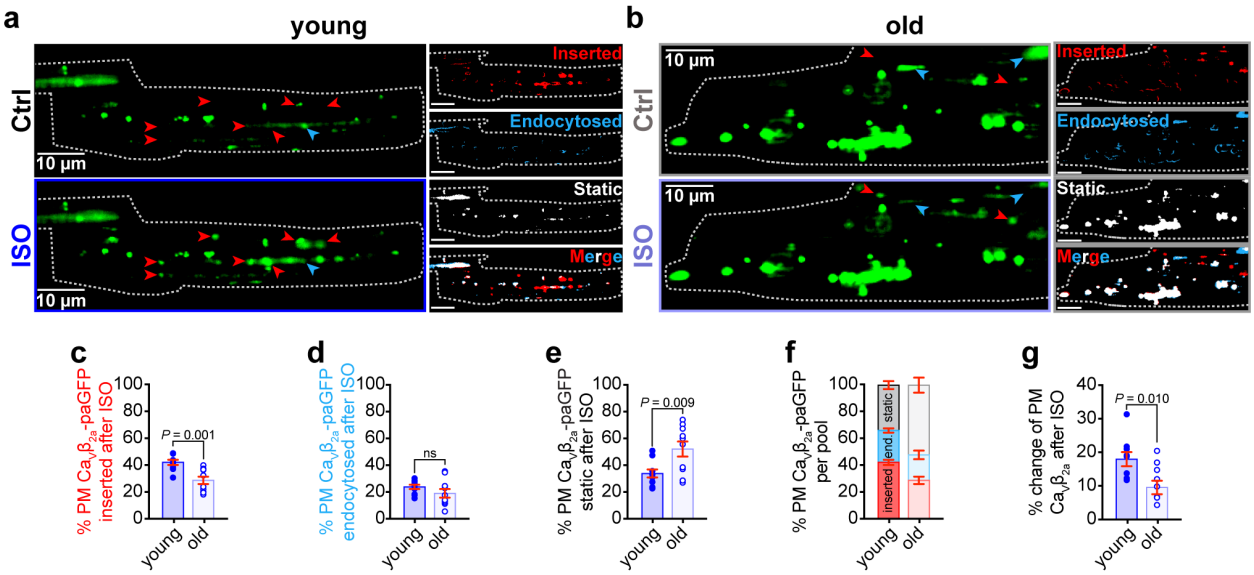

Figure 3. Dynamic TIRF imaging reveals age-associated trafficking deficits of $Ca_V1.2$.

a and **b**, Representative TIRF images of transduced $Ca_v\beta_{2a}$-paGFP young (**a**) and old (**b**) ventricular myocytes before (*top*) and after ISO (*bottom*). Channel populations that were inserted (red), endocytosed (blue), or static (white) during the ISO treatment are represented to the *right*. **c-e**, dot-plots summarizing the quantification of inserted (**c**), endocytosed (**d**), and static (**e**) $Ca_v\beta_{2a}$-paGFP populations. **f**, is a compilation of the data in c, d, and e to show the relative % of the channel pool that is inserted, endocytosed, and static. **g**, is a summary plot showing the net % change of plasma membrane $Ca_v\beta_{2a}$-paGFP after ISO for each cohort of young (N = 3, n = 10) and old (N = 3, n = 10) myocytes. Data were analyzed for statistical analysis using unpaired Student's t-tests.

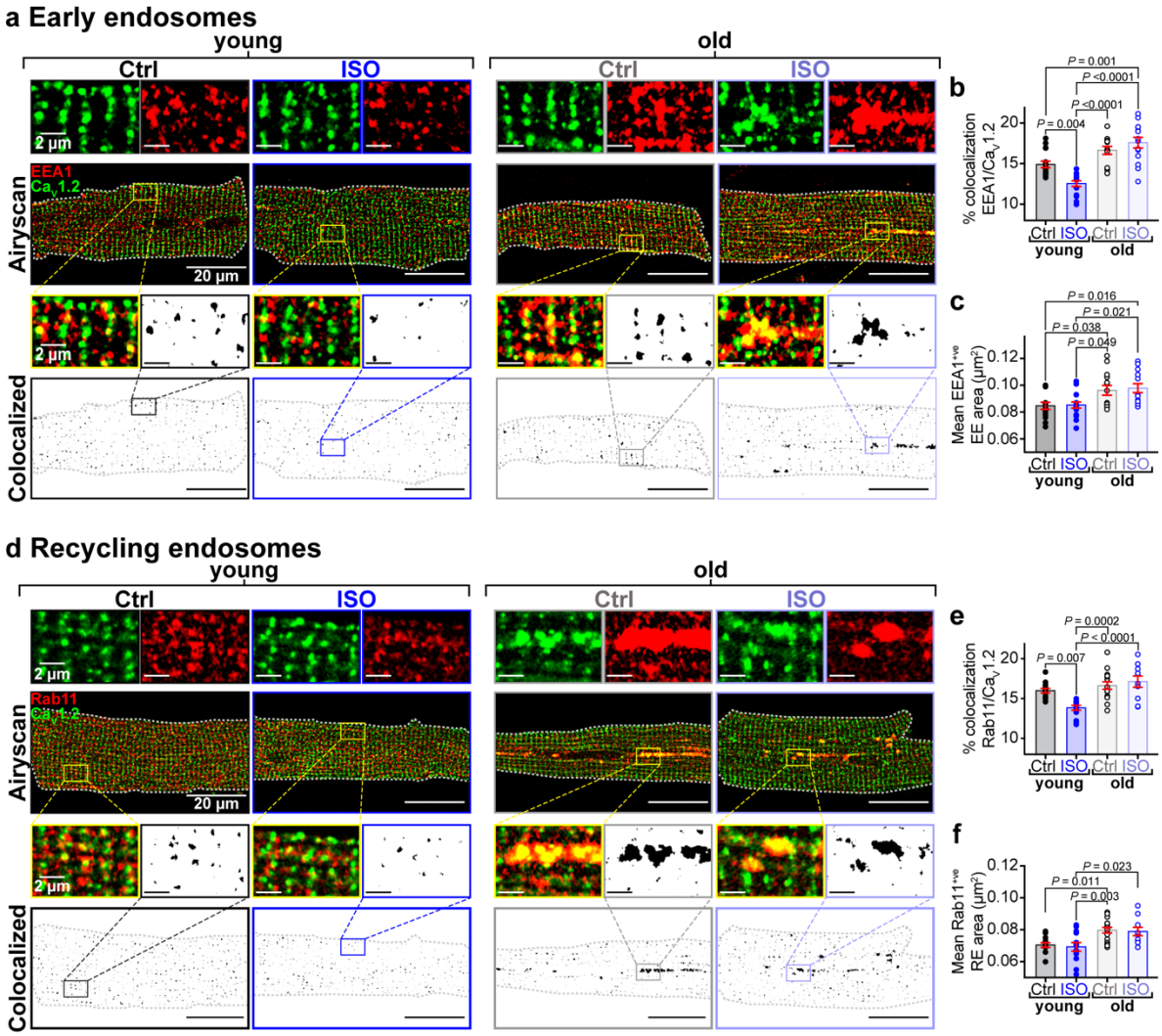

Figure 4. Aging impairs *β*-AR-stimulated $Ca_V1.2$ recycling. a, Airyscan super-resolution images of $Ca_V1.2$ and EEA1 immuno-stained myocytes with and without ISO. *Bottom:* Binary colocalization maps show pixels in which $Ca_V1.2$ and EEA1 completely overlapped. **b**, dot-plots summarizing % colocalization between EEA1 and $Ca_V1.2$, and **c**, EEA1 positive endosome areas in young (control: $N = 3$, $n = 16$; ISO: $N = 3$, $n = 16$) and old (control: $N = 3$, $n = 14$; ISO: $N = 3$, $n = 14$) myocytes. **d-f,** same layout for myocytes co-stained for $Ca_V1.2$ and Rab11 recycling endosomes in young (control: $N = 3$, $n = 13$; ISO: $N = 3$, $n = 13$) and old (control: $N = 4$, $n =16$; old ISO: $N = 3$, $n = 10$) myocytes. Data were analyzed using two-way ANOVAs with post-hoc Tukey's multiple comparison tests.

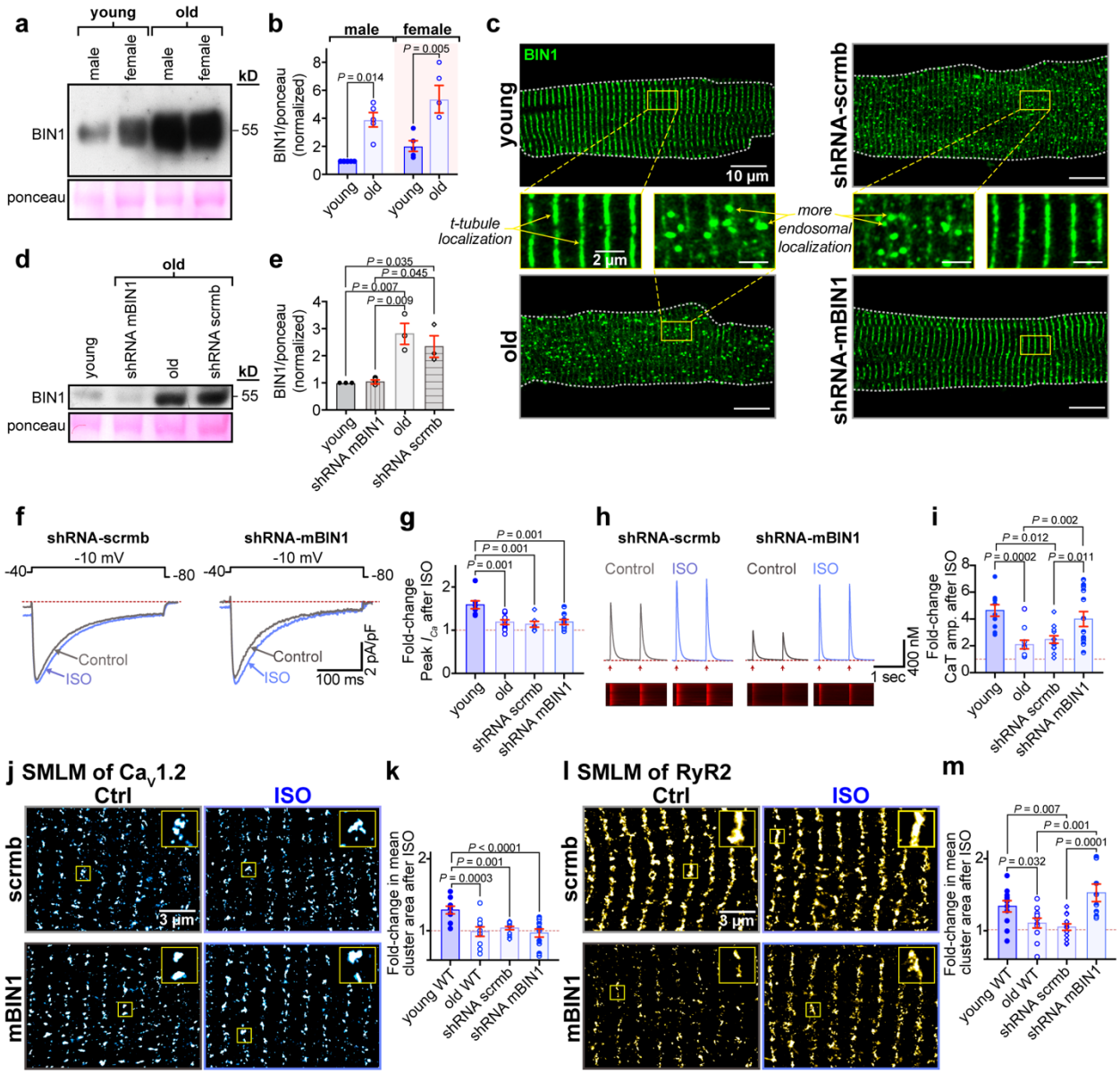

728

729 **Figure 5. BIN1 knockdown restores *β*-AR augmentation of Ca^{2+} transients and RyR2**
730 **clustering dynamics. a**, western blot of BIN1 expression in whole heart lysates from young and
731 old mice. Ponceau was used for normalization. **b**, histogram showing normalized BIN1 levels
732 relative to young male (*N* = 5, average of 1-2 replicates). **c**, representative Airyscan images of
733 young, old, and old transduced myocytes immunostained against BIN1. **d**, western blot of BIN1
734 expression in whole heart lysates from: young, old, shRNA-mBIN1 or shRNA-scrmb transduced
735 mice. Ponceau was used for normalization. **e**, histogram showing normalized BIN1 levels relative

736 to young (*N* = 3, average of 1 - 3 replicates). **f**, representative whole-cell currents from shRNA-
737 scrmb and shRNA-mBIN1 myocytes before and during ISO application. **g**, fold change in peak I_{Ca}
738 with ISO in young, old, shRNA-scrmb (*N* = 3, *n* = 7) and shRNA-mBIN1 (*N* = 3, *n* = 9) myocytes.
739 **h**, representative Ca^{2+} transients recorded from old shRNA-scrmb and shRNA-mBIN1 myocytes
740 before and after ISO. **i**, fold increase after ISO from young, old, shRNA-scrmb (*N* = 3, *n* = 12) and
741 shRNA-mBIN1 (*N* = 5, *n* = 13) myocytes. **j**, SMLM localization maps showing $Ca_V1.2$ channel
742 localization on t-tubules of myocytes from old shRNA-scrmb and shRNA-mBIN1, with or without
743 ISO-stimulation. Regions of interest are highlighted by yellow boxes. **h**, fold change in mean
744 $Ca_V1.2$ channel cluster area with ISO in the old shRNA-scrmb (control: *N* = 3, *n* = 14; ISO: *N* = 3,
745 *n* = 13) and shRNA-mBIN1 myocytes (control: *N* = 3, *n* = 12; ISO: *N* = 3, *n* = 11). **l** and **m**, show
746 the same layout for RyR2 immunostained old shRNA-scrmb (control: *N* = 3, *n* = 12; ISO: *N* = 3, *n*
747 = 13) and shRNA-mBIN1 myocytes (control: *N* = 3, *n* = 9; ISO: *N* = 3, *n* = 8). Old and young data
748 points in g, i, k and m are reproduced from data in Figs. 1b, 1e, 2b and 2d respectively. Statistical
749 analysis was performed on data in b using a two-way ANOVA, and data in e, g, i, k and m using
750 one-way ANOVAs.
751

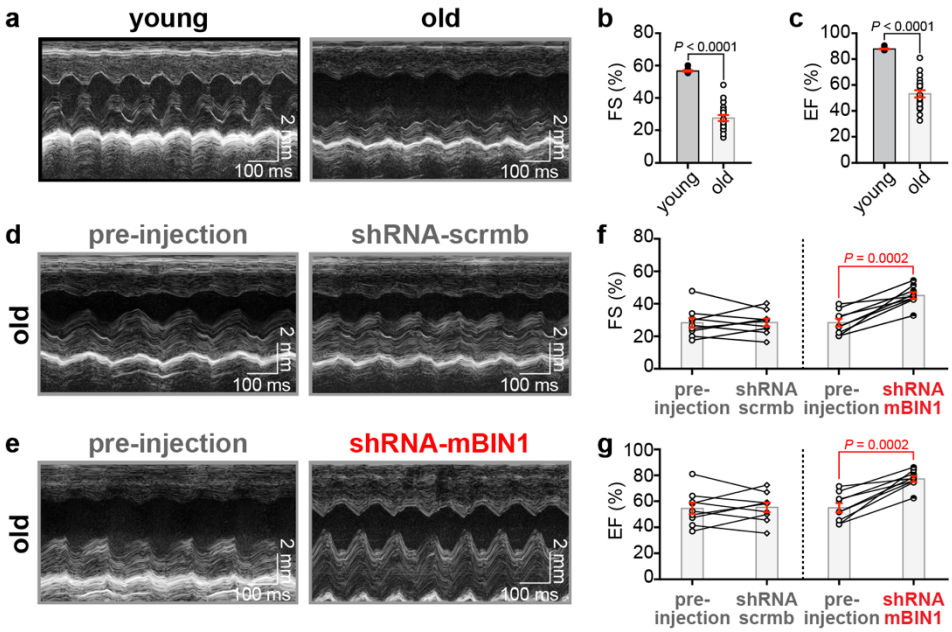

752

753

754 **Figure 6. BIN1 knockdown improves cardiac contractility in old mice. a**, representative M-
755 mode echocardiogram images from conscious young and old mice. Summary dot-plots showing
756 **b,** fractional shortening and **c,** ejection fraction in young (*N* = 11) and old (*N* = 20) mice are shown.
757 **d** and **e,** representative M-mode echocardiogram images from conscious old mice before (*left*)
758 and two-weeks after RO-injection (*right*) of shRNA-scrmb (**d**) and shRNA-mBIN1 (**e**). Summary
759 dot-plots for **f,** fractional shortening and **g**, ejection fraction showing paired results before and
760 after RO-injection for shRNA-scrmb (*N* = 9) and shRNA-mBIN1 (*N* = 9) groups are displayed.
761 Unpaired Student's t-tests were performed on data displayed in b and c. Paired Student's t-tests
762 were performed on data displayed in f and g.

763

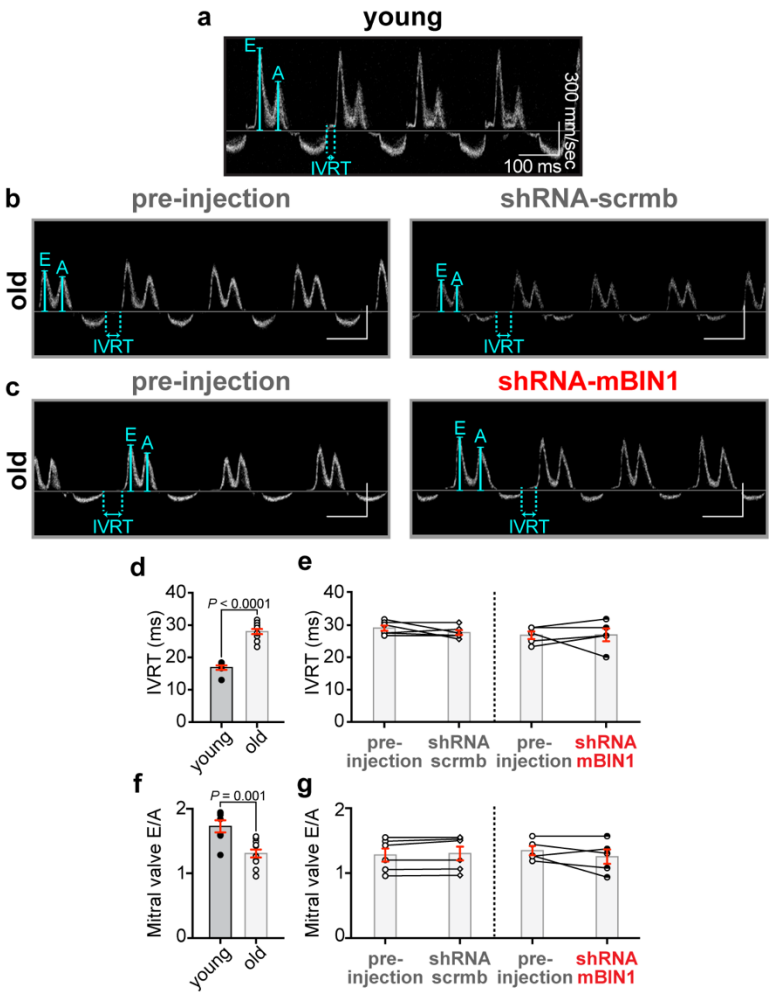

764

765 **Figure 7. BIN1 knockdown does not recover age-related diastolic dysfunction.**
766 Representative pulsed-wave (PW) doppler images from unconscious young (**a**) and old mice
767 before (left) and two-weeks after RO-injection (right) of shRNA-scrmb (**b**) and shRNA-mBIN1 (**c**).
768 Summary dot-plots for young (*N* = 7) and old (*N* = 11) mice, and paired results before and after
769 RO-injection of old mice with shRNA-scrmb (*N* = 6) and shRNA-mBIN1 (*N* = 5) for the following
770 diastolic measurements are displayed: **d** and **e**, isovolumetric relaxation time (IVRT) and, **f** and
771 **g,** mitral valve E/A ratio (MV E/A). Unpaired Student's t-tests were performed on data displayed
772 in d and f. Paired Student's t-tests were performed on data displayed in e and g.

773

774

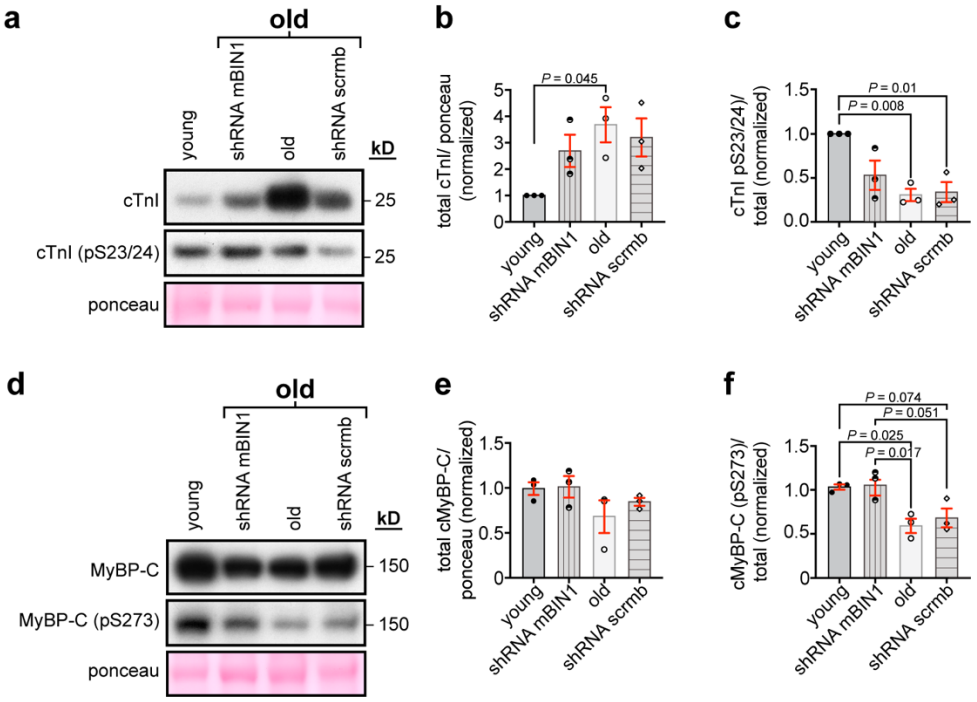

Figure 8. Myofilament Ca^{2+} sensitivity is altered in aging. a, western blot of total and pS23/24 cTnI expression in whole heart lysates from young, old, shRNA-mBIN1 or shRNA-scrmb transduced mice. Ponceau was used for normalization. **b**, histogram showing normalized total cTnI levels relative to young (*N* = 3, average of 3 replicates). **c**, histogram showing cTnI pS23/24 normalized to total cTnI relative to young (*N* = 3, average of 2-3 replicates). **d**, western blot of total and pS273 cMyBP-C expression in whole heart lysates from young, old, shRNA-mBIN1 or shRNA-scrmb transduced mice. Ponceau was used for normalization. **e**, histogram showing normalized total cMyBP-C levels relative to young (*N* = 3, average of 2-5 replicates). **f**, histogram showing cMyBP-C pS273 normalized to total cMyBP-C relative to young (*N* = 3, average of 2-5 replicates).